International Journal of Remote Sensing
Vol. 28, No. 12, 20 June 2007, 2753–2775

Production of Landsat ETM+ reference imagery of burned areas within Southern African savannahs: comparison of methods and application to MODIS

A. M. S. SMITH*†, N. A. DRAKE‡, M. J. WOOSTER‡, A. T. HUDAK§, Z. A. HOLDEN† and C. J. GIBBONS¶

†Department of Rangeland Ecology and Management, University of Idaho, Moscow, ID 83844, USA

‡Department of Geography, King's College London, London WC2R 2LS, UK

§Rocky Mountain Research Station, USDA Forest Service, Moscow, ID 83843, USA

¶Peak District National Park Authority, Bakewell DE45 1AE, UK

(*Received 19 May 2006; in final form 2 August 2006*)

Accurate production of regional burned area maps are necessary to reduce uncertainty in emission estimates from African savannah fires. Numerous methods have been developed that map burned and unburned surfaces. These methods are typically applied to coarse spatial resolution (1 km) data to produce regional estimates of the area burned, while higher spatial resolution (<30 m) data are used to assess their accuracy with little regard to the accuracy of the higher spatial resolution reference data. In this study we aimed to investigate whether Landsat Enhanced Thematic Mapper (ETM+)-derived reference imagery can be more accurately produced using such spectrally informed methods. The efficacy of several spectral index methods to discriminate between burned and unburned surfaces over a series of spatial scales (ground, IKONOS, Landsat ETM+ and data from the MOderate Resolution Imaging Spectrometer, MODIS) were evaluated. The optimal Landsat ETM+ reference image of burned area was achieved using a charcoal fraction map derived by linear spectral unmixing (k=1.00, a=99.5%), where pixels were defined as burnt if the charcoal fraction per pixel exceeded 50%. Comparison of coincident Landsat ETM+ and IKONOS burned area maps of a neighbouring region in Mongu (Zambia) indicated that the charcoal fraction map method overestimated the area burned by 1.6%. This method was, however, unstable, with the optimal fixed threshold occurring at >65% at the MODIS scale, presumably because of the decrease in signal-to-noise ratio as compared to the Landsat scale. At the MODIS scale the Mid-Infrared Bispectral Index (MIRBI) using a fixed threshold of >1.75 was determined to be the optimal regional burned area mapping index (slope=0.99, r^2=0.95, SE=61.40, y=Landsat burned area, x=MODIS burned area). Application of MIRBI to the entire MODIS temporal series measured the burned area as 10 267 km^2 during the 2001 fire season. The char fraction map and the MIRBI methodologies, which both produced reasonable burned area maps within southern African savannah environments, should also be evaluated in woodland and forested environments.

*Corresponding author. Email: alistair@uidaho.edu

International Journal of Remote Sensing
ISSN 0143-1161 print/ISSN 1366-5901 online
http://www.tandf.co.uk/journals
DOI: 10.1080/01431160600954704

1. Introduction

Since the early 1980s the importance of wildfires as a driver of global climate change has been amply demonstrated (Seiler and Crutzen 1980, Levine 1990, French *et al.* 2004). Current estimates suggest that global biomass burning may, on average, account for something like 40% of total carbon monoxide and carbon dioxide loads emitted to the atmosphere (Andreae and Merlet 2001, Kasischke and Bruhwiler 2003), although the actual proportion will vary considerably in response to climate anomalies such as El Nino (Goldammer 1999, Slegert *et al.* 2001). Biomass burning in tropical savannahs and grasslands is thought to constitute the single largest source of pyrogenic emissions (Crutzen and Andreae 1990, Hao *et al.* 1990, Andreae and Merlet 2001), with up to 20% of these are thought to result from southern Africa (Hao and Liu 1994, Coffer *et al.* 1996, Scholes *et al.* 1996). Regional emissions assessments typically rely on maps of burned (or 'fire affected') area, within which measures of fuel load, fire behaviour and emissions characteristics are then assessed to calculate emissions totals. For tropical savannahs and grasslands, the uncertainty associated with estimates of burned area is often considered the largest source of error in such calculations because of their relatively homogeneous fuels loads and fire characteristics (Pereira *et al.* 1999, French *et al.* 2004). Accurate burned area maps are therefore necessary to minimize uncertainty in such estimates. A considerable amount of research has been conducted to produce regional maps of burned area within African savannahs, with studies focusing on central Africa (Frederikson *et al.* 1990, Eva and Lambin 1998), southern Africa (Roy *et al.* 1999, Smith *et al.* 2002, Hudak and Brockett 2004), and the entire continent (Barbosa *et al.* 1998, Grégoire *et al.* 2003).

Our understanding of the reflectance properties of burned areas has increased dramatically over the past few years and we are now beginning to understand the factors that control their spectral response (Lentile *et al.* 2006). The replacement of healthy vegetation (healthy or senesced) by charcoal lowers visible (0.5–0.7 μm) to near-infrared (NIR) (0.8–1.2 μm) reflectance, while the increase in both charcoal and soil cover over healthy vegetation raises both short-wave infrared reflectance (SWIR) (2.0–2.5 μm) and surface temperature (Trigg and Flasse 2000, Stroppiana *et al.* 2002). The SWIR reflectance can decrease when charcoal or soils replace senesced vegetation (Eva and Lambin 1998). At localized points during intense fires, the visible to NIR reflectance may in fact increase because of the production of white mineral ash (Landman 2003, Roy and Landman 2005, Smith and Hudak 2005), although this effect is diminished by spatial averaging and is very unlikely to be detectable at the scale of Landsat or coarser spatial resolution sensors (Smith *et al.* 2005*b*).

The reflective and thermal characteristics of burned areas have led to the use of various spectral indices defined in table 1 for burned area discrimination, including the Normalized Difference Vegetation Index (NDVI; Rouse *et al.* 1974), the Global Environmental Monitoring Index (GEMI; Barbosa *et al.* 1999), the Burned Area Index (BAI; Chuvieco *et al.* 2002) and the Soil Adjusted Vegetation Index (SAVI; Chuvieco *et al.* 2002). Each of these indices uses the property of an observed NIR reflectance decrease to assist in discrimination between burned and unburned savannah surfaces. The concurrent increase in SWIR reflectance is used in certain of the indices, such as the Mid-Infrared Bispectral Index (MIRBI; Trigg and Flasse 2001), the Normalized Burn Ratio (NBR; Lopez-Garcia and Caselles 1991) and the Char Soil Index (CSI; following indices tested by Smith *et al.* 2005*b*). In a recent study, Holden *et al.* (2005) further modified the vegetation index number 3 (VI-3)

Table 1. Definition of the different indices used in the paper.

Equation	Index	Reference
BAI	$[(G_r-\rho_r)^2+(G_{NIR}-\rho_{NIR})^2]^{-1}$	Chuvieco *et al.* (2002)
CSI	$\rho_{NIR}/(\rho_{SWIR})$	Smith *et al.* (2005*b*)
EVI	$2.5(\rho_{NIR}-\rho_r)/[(\rho_{NIR}+6\rho_r)-7.5\rho_b+1]$	Huete *et al.* (1997)
GEMI	$n(1-0.25n)-(\rho_r-0.125)/(1-\rho_r)$	Pinty and Verstraete (1992)
MIRBI	$10\rho_{SWIR}-9.8\rho_{LNIR}+2.0$	Trigg and Flasse (2001)
NBR	$(\rho_{NIR}-\rho_{SWIR})/(\rho_{NIR}+\rho_{SWIR})$	Key and Benson (2002)
NDVI	$(\rho_{NIR}-\rho_r)/(\rho_{NIR}+\rho_r)$	Rouse *et al.* (1974)
SAVI	$(\rho_{NIR}-\rho_r)(1+L)/(\rho_{NIR}+\rho_r+L)$	Barbosa *et al.* (1999)
VI6T	$(\rho_{NIR}-S_{TIR})/(\rho_{NIR}+S_{TIR})$	Holden *et al.* (2005)
NBRT	$[\rho_{NIR}-(\rho_{SWIR}S_{TIR})]/[\rho_{NIR}+(\rho_{SWIR}S_{TIR})]$	Holden *et al.* (2005)
CSIT	$\rho_{NIR}/(\rho_{SWIR}S_{TIR})$	This study
NDVIT	$[\rho_{NIR}-(\rho_rS_{TIR})]/[\rho_{NIR}+(\rho_rS_{TIR})]$	This study
SAVIT	$[\rho_{NIR}-(\rho_rS_{TIR})](1+L)/[\rho_{NIR}+(\rho_rS_{TIR})+L]$	This study

BAI classified with a threshold=mean−1 standard deviation.
In GEMI, $n=[2(\rho_{NIR}{}^2-\rho_r{}^2)+1.5\rho_{NIR}+0.5\rho_r]/(\rho_{NIR}+\rho_r+0.5)$.
BAI, Burned Area Index; CSI, Char Soil Index; EVI, Enhanced Vegetation Index; GEMI, Global Environmental Monitoring Index; MIRBI, Mid-Infrared Bispectral Index; NBR, Normalized Burn Ratio; NDVI, Normalized Difference Vegetation Index; SAVI, Soil Adjusted Vegetation Index; VI6T, Vegetation Index Number 6 Thermal; NBRT, NBR-Thermal; CSIT, CSI-Thermal; NDVIT, NDVI-Thermal; SAVIT, SAVI-Thermal.
ρ_b=sensor blue reflectance (TM band 1); ρ_r=sensor red reflectance (TM band 3); G_r=ground measured red reflectance; ρ_{NIR}=sensor NIR reflectance (TM band 4); G_{NIR}=ground measured NIR reflectance; ρ_{LNIR}=sensor long near-infrared reflectance (TM band 5); ρ_{SWIR}=sensor SWIR reflectance (TM band 7); S_{TIR} denotes scaled brightness temperature=TIR value divided by 10 000; L=soil constant set to 0.5.

and NBR indices to include thermal infrared (TIR) data from Landsat Enhanced Thematic Mapper (ETM+) band 6 (VI-6T, NBRT), highlighting the utility of the increase in surface temperature generally observed post-fire. Finally, burned pixels can to some extent be distinguished from other surfaces in the middle IR (MIR) spectral region, and versions of the NDVI and GEMI indices have been derived that replace use of the red spectra band by the reflectance component of the MIR (VI3 and GEMI-3; Kaufman and Remer 1994, Barbosa *et al.* 1999).

Several of the more recent indices such as the Enhanced Vegetation Index (Huete *et al.* 1997, Chen *et al.* 2004), MIRBI (Trigg and Flasse 2001) and VI6T (Holden *et al.* 2005) have yet to be fully evaluated, in particular with respect to the utility when analysing satellite imagery of southern African savannahs. Prior analysis of the more established indices applied to data from multiple coarse spatial resolution sensors has highlighted several sources of error. The classification of low albedo surfaces (e.g. water and tilled soil) as burned surfaces is common with BAI, NDVI, VI3 and GEMI (Eva and Lambin 1998, Pereira 1999, Chuvieco *et al.* 2002). Furthermore, small amounts of unburned senesced vegetation are often left behind by fires and these areas are often misclassified as savannah woodland, rather than burnt areas, when using NDVI-based approaches (Frederikson *et al.* 1990, Razafimpanilo *et al.* 1995). Sparsely vegetated areas may be similarly misclassified by SAVI (Chuvieco *et al.* 2002).

As an alternative to spectral indices, a few burnt area mapping studies have used approaches that attempt to estimate the proportion of a pixel affected by fire (Caetano *et al.* 1996, Cochrane and Souza 1998, Shabanov *et al.* 2005, Vafeidis and Drake 2005). A common approach is linear spectral unmixing (also known as spectral mixture

analysis (SMA) or linear mixture modelling). A common source of commission error in linear spectral unmixing studies arises from the presence of dark soils or previously burned areas within an unburned pixel (Caetano *et al.* 1996, Shabanov *et al.* 2005). A further source of error in the form of omission errors can arise at boundary pixels (Caetano *et al.* 1996, Vafeidis and Drake 2005). In addition, surfaces with excessive shadowing, such as those in complex terrain and heavily forested areas, may also contribute to commission errors (Cochrane and Souza 1998).

2. Objectives

The current study seeks to comprehensively evaluate the efficacy of index-based methods of burned area mapping in southern African savannahs. It is conducted at four discrete spatial scales (ground, IKONOS, Landsat ETM+ and MODIS) and the aim is to select the most appropriate methods for the production of a reference map with the Landsat sensor and the production of regional burned area estimates using data from the MODIS sensor.

To achieve these objectives, detailed accuracy assessment of the resulting burned area maps is required. This has generally been undertaken by comparison to higher spatial resolution reference imagery (e.g. Eva and Lambin 1998, Barbosa *et al.* 1999, Smith *et al.* 2002, Brivio *et al.* 2003, Silva *et al.* 2003). Typically supervised or unsupervised multispectral classification methods have been applied to high spatial resolution data (e.g. 30 m ETM+ imagery) to produce the reference datasets, but the accuracy of the reference maps themselves are seldom independently evaluated (Eva and Lambin 1998, Barbosa *et al.* 1999, Chuvieco *et al.* 2002, Smith *et al.* 2002, Silva *et al.* 2003, Hudak and Brockett 2004). Furthermore, these studies generally do not incorporate the fire-specific spectral information that has been developed and applied to the coarse spatial resolution datasets.

Here we address these limitations by adopting a general upscaling approach involving the spectral analysis of burned savannah surfaces at four spatial scales:

(i) Analysis of *in situ* spectral data to evaluate the efficacy of the various index-based methods. The analysis area is 11 cm^2 and can provide information on how fire affects the fine-scale spectral characteristics of the savannah surfaces, which enables a fuller understanding of the mechanistic links between fire heat transfer and the impacts on the biogeochemical and water cycles relevant to soils and vegetation (Smith *et al.* 2005*b*, Lewis *et al.* 2006).

(ii) Mapping boundaries of selected fires from a ground truth Global Positioning System (GPS)/photograph record and coincident Landsat ETM+ imagery to accurately identify burnt and unburnt pixels. The analysis area varies from 900 m^2 to hundreds of km^2 and has the potential to provide information on how the fire affects landscape-scale processes, such as measures of the burn severity (van Wagtendonk *et al.* 2004, Lentile *et al.* 2006), which are of interest to land management personnel.

(iii) Comparing a series of burned area mapping methods applied to Landsat ETM+ data with finer spatial resolution data from IKONOS of a similar neighbouring region. This represents the intermediate scale between (i) and (ii).

(iv) Assessment of a series of burned area mapping methods to the MODIS data and comparisons with coincident Landsat ETM+ imagery. The analysis area varies from 0.25 km^2 to >1000 km^2 and has the potential to provide

information on regional to global processes, such as regional pyrogenic emission estimates.

3. Study area, data and preprocessing

The primary study site was Chobe National Park (figure 1(*a*)), northeastern Botswana (upper left: 17.65°S, 24.21°E; lower right: 19.47°S, 26.30°E), an area subject to annual large-scale fires (Smith 2004, Smith *et al.* 2005*a*). A field campaign (12–25 October 2001) resulted in the collection of representative field spectra and

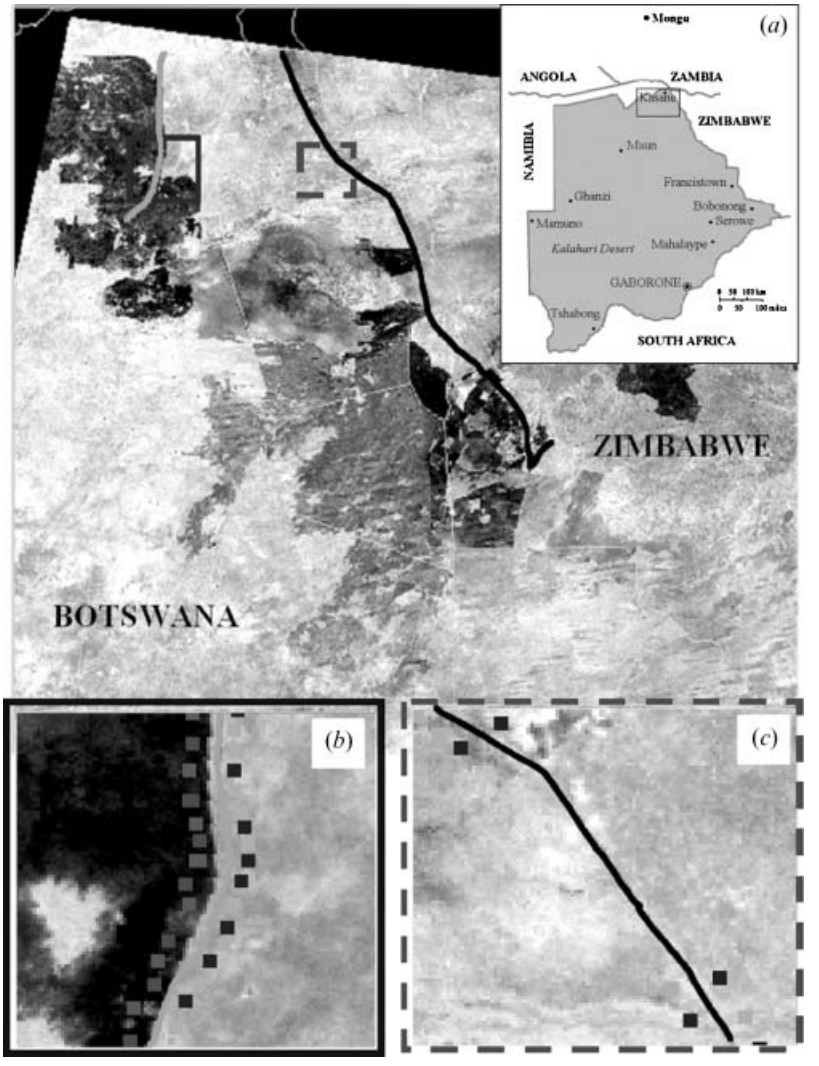

Figure 1. (*a*) The location of Chobe National Park, northern Botswana. Landsat 7 ETM+ image of north-eastern Botswana showing large (darker) areas of burned savannah grassland and woodland, overlain by two vector files denoting the transects made in the field on 19 and 20 October 2001. (*b*) Magnified view of transect 1, showing examples of pixels selected as burned (left) and unburned (right). (*c*) Magnified view of transect 2, showing examples of pixels selected as unburned.

surveys of fire boundaries coincident with an ETM+ image acquisition on 8 October 2001 (Smith *et al.* 2005*b*). A temporal series of 36 MODIS 1B scenes (1 June to 1 November 2001) surrounding (both spatially and temporally) the ETM+ image data was also collected. A second burned area ETM+ scene was acquired almost simultaneously with an IKONOS image (figure 3: 16 and 17 August 2000) for burns in Mongu, western Zambia (centre: 15.44°S, 23.25°E; less than 350 km north of Chobe National Park). No temporally coincident IKONOS and ETM+ match-ups were available for northern Botswana, and western Zambia was chosen as the most similar location where field information and coincident imagery from both sensors were available (collected as part of the Southern African Fire Atmosphere Regional Initiative, SAFARI-2000; see Hely *et al.* 2003*a*,*b*). Data from Landsat ETM+ band 6 were calibrated to brightness temperature units (K), while both the IKONOS and ETM+ optical bands were calibrated into top-of-atmosphere (TOA) spectral reflectance using the standard Landsat radiance and reflectance conversion equations (see Eva and Lambin 1998, Chander and Markham 2003, Flemming 2003). The MODIS 1B data were similarly converted into TOA reflectance using the gain and offsets contained within the metadata of the MODIS hdf file.

The Chobe Landsat ETM+ imagery was atmospherically corrected by using the empirical line method (Kruse *et al.* 1990, Smith and Milton 1999). This was achieved by selecting the known surface locations within the imagery using the ENVI (RSI, Boulder, CO, USA) software package and matching these to the field-collected spectral reflectance data of those cover types. A GER-3700 field spectroradiometer with an 11 cm^2 field of view was used to collect these spectra, with details of the methodology provided in Smith *et al.* (2005*b*). In addition to unburned cover types (senesced vegetation, soils, green tree leaves), spectral examples of post-fire savannah surfaces (white ash, charcoal, and mixed ash) were collected from instrumented plots within Chobe National Park (Smith *et al.* 2005*b*).

Prior to application, the full-range spectroradiometer data were converted into the sensor's band equivalent reflectance (Trigg and Flasse 2001) to allow a single value corresponding to each individual sensor band. This is necessary because ENVI (and other) software packages require that both the imagery and spectra contain an equal number of bands. Following Trigg and Flasse (2000) and Smith *et al.* (2005*b*), this was achieved by convolving each spectra with the spectral response function of each sensor band. The software package then calculated for each band, the line and intercept between the sensor's band radiance and the surface reflectance using each surface type as a point (green vegetation, senesced vegetation, and soil). This line and intercept is then applied to convert the band radiance to surface reflectance. The Mongu Landsat ETM+ and IKONOS imagery were also atmospherically corrected using the empirical line method by use of the Chobe field spectra, which were representative of both areas (senesced grasses, green tree leaves, grey–brown soil). GPS-derived coordinates, *in situ* documentation and photographs of vegetative (senesced and green) and bare soil areas identified during the SAFARI-2000 fieldwork campaign were used to identify endmember pixels within the Mongu imagery (Smith 2004). Although we acknowledge that the dominant grass species types between Mongu and Chobe were different, the spectral reflectance curves of senesced vegetation (and similarly green vegetation) for different species have been shown to be broadly similar (e.g. Elvidge 1990, Smith *et al.* 2005*b*). These broad similarities are further pronounced with the band equivalent reflectance conversion, as each spectral response function was reduced to six band-averaged points.

Furthermore, field observations verified that the senesced grass vegetation at the Mongu sites was fully senesced, while the Mongu green vegetation corresponded with green wooded areas. As such, we submit that seasonal differences and thus potential sources of error that could have resulted in using spectral data from the mid-October Chobe site within the mid-August Mongu imagery were minimized.

Two field GPS transects (figure 1: collected 19–20 October 2001) crossing a patchwork of burned and unburned surfaces were used to produce 250 groups of 4×4 pixels in the georegistered ETM+ image that were either burned or unburned at the time of image acquisition (figures 1(*b*) and 1(*c*)). The first transect (figure 1(*b*)) was within Chobe National Park, while the second transect (figure 1(*c*)) was outside the park and followed the Botswana/Zimbabwe border. Half the pixels were used as training data for a maximum likelihood (Richards and Jia 1999) classification of the ETM+ image, while the remaining pixels were used to confirm the accuracy of this classification. The training data were further used to define thresholds in each subsequent classification method. An additional supervised classification of the ETM+ imagery was implemented using the parallelepiped (Hudak and Brockett 2004) classifier. In each classification, all Landsat ETM+ optical bands were used in the classification. The supervised classifications produced binary burned/unburned maps.

4. Image processing

4.1 *Spectral index methods*

The indices presented in table 1 were applied to the ETM+ imagery and pixels classed as burned or unburned using an appropriate threshold. Within the burned area classification literature, a large selection of different approaches have been adopted to set automatic classification thresholds of methods that use spectral indices (Fernandez *et al.* 1997, Barbosa *et al.* 1999, Roy *et al.* 1999, Nielsen *et al.* 2002, Vafeidis and Drake 2005). For the purpose of this study, we sought to explore the most stringent classification test. We thus calculated the mean (μ) and standard deviation (σ) of the index from the burned pixel training dataset collected from the analysis of the transects and (following Barbosa *et al.* (1999), Holden *et al.* (2005), and others) all pixels in the image were defined as burned if their index value fell within the range $\mu \pm 2\sigma$. For MIRBI and BAI we used the fixed thresholds reported in Trigg and Flasse (2001) and Chuvieco *et al.* (2002). The MIRBI technique, when applied by Trigg and Flasse (2001) to savannahs in north-eastern Namibia, determined surfaces as burned when MIRBI values were >1.7. As our study was within 400 km of this prior study area and in a similar savannah environment, we used this threshold as a starting basis but also investigated sequential increments of 0.05 about this value.

4.2 *Unsupervised classification*

Unsupervised classification was also conducted by means of the ISODATA algorithm (Ball and Hall 1965). Four to 10 classes and four iterations were used with the latter approach, resulting in seven final classes. Rather than visually defining each separate ISODATA output class as burned or unburned, we followed a similar objective approach to that applied to the spectral index methods. The mean and standard deviation of the ISODATA output class values were calculated for the set of pixels contained within the burned pixel training dataset collected from the

analysis of the transects. The pixels were then classed as burned if their ISODATA output class value fell within two standard deviations of the mean of the training data pixels. In this classification, all Landsat ETM+ optical bands were used.

4.3 *Linear spectral unmixing*

Linear spectral unmixing (Settle and Drake 1993, Wessman *et al.* 1997, Drake *et al.* 1999) was applied to the Landsat ETM+ and MODIS imagery using the field-derived spectral endmembers of charcoal, green vegetation and senesced vegetation. Extensive linear spectral unmixing theory exists in the literature (e.g. Drake and White 1991, Drake *et al.* 1999, Sa *et al.* 2003, Shabanov *et al.* 2005). Spectral unmixing was performed using the algorithm contained within IDL/ENVI version 4.2, with the 'sum to 1' constraint applied (Drake *et al.* 1999). Although, with this constraint applied, all the proportions within a pixel will sum to 100%, it remains possible for both negative proportions and proportions exceeding 100% to occur.

The central assumption of linear spectral unmixing is that each surface component within a pixel is sufficiently large such that no multiple scattering exists between the components (Drake *et al.* 1999). This scattering approximation is valid when the pixel size exceeds the typical 'patch' or component being sensed (Qin and Gerstl 2000) and, importantly, is valid for charcoal and white ash mixtures within southern African savannahs (Smith *et al.* 2005*b*). In an attempt to minimize commission errors associated with small fractions of non-burned surfaces (water, soil, etc.) appearing in the final burned area map, a pixel was only considered as burned if the charcoal fraction within it exceeded a predetermined threshold. This threshold can be chosen arbitrarily, and a series of mixture-model derived burned area maps using charcoal thresholds from >100% to >45%, in increments of 5%, were derived.

4.4 *Accuracy assessment*

4.4.1 Spectral separability of burnt areas. Following Pereira (1999), the underlying spectral separability of the burned and unburned pixels was assessed at all spatial scales (i.e. ground data, ETM+ and MODIS) using the *M*-statistic (equation (1)), which exceeds 1 when the two classes exhibit moderate separability:

$$M = (\mu_u - \mu_b)/(\sigma_u - \sigma_b) \quad (1)$$

where μ_u and σ_u are, respectively, the mean and standard deviation of the unburned surfaces, and μ_b and σ_b are, respectively, the mean and standard deviation of the burned surfaces. This statistic, originally presented by Kaufman and Remer (1994), allows the determination of which burned area mapping indices provide reasonable discrimination (i.e. $M>1$). At the scale of the ground-based measurements, the mean and standard deviation of each index was calculated using the simulated Landsat ETM+ reflectance data. At the ETM+ and MODIS scales the training pixels described above were used to calculate the *M*-statistic.

4.4.2 Thematic map accuracy assessment. The *M*-statistic cannot be applied to evaluate the utility of the classification and linear spectral unmixing methods. Instead, we used measures of classification accuracy assessment, and in particular the kappa statistic, k (Fuller and Falk 2001, Hann *et al.* 2003), and the overall accuracy, a, calculated by comparing the classified images with the validation pixels

identified in the ground survey. Identification of the method with the highest values of k and a determined which approach was most accurate.

The very high spatial resolution of IKONOS means that it can provide a suitable reference image to evaluate the accuracy of the ETM+ classification. The IKONOS image was classified using a maximum likelihood classifier, chosen using a stratified random sample design whereby pixels were located randomly within the main vegetation types identified during fieldwork performed during the SAFARI 2000 field campaign (see Hely *et al.* 2003*a*,*b*). We classified the Mongu Landsat ETM+ image using the best Landsat reference image production method identified by the analysis of the Chobe datasets. Information on the omission and commission errors for the Landsat method selected for the burned area classification is presented during the Chobe Landsat analysis. Assessment of the classification bias was then achieved by analysing the regression statistics between the IKONOS (dependent variable) and Landsat (independent variable) burned area measures; for example, the slope of the regression line (<1=overestimation, >1=underestimation), the coefficient of determination (r^2) and the standard error (SE). Following prior studies (Eva and Lambin 1998, Smith *et al.* 2002), both the Landsat and IKONOS images in figures 3(*a*) and 3(*c*), which cover the same spatial extent, were divided into 16 regular grid squares and the burned area produced from each classification within each grid square calculated.

4.5 *Selection of the MODIS regional mapping method*

Following production of the best method to produce the Landsat reference map of burned area, we use the resultant map to determine the accuracy of the MODIS burnt area estimates. This is achieved by comparing coincident MODIS and Landsat burned area maps in the same manner as for the ETM+/IKONOS comparison outlined above. The area burned over the entire fire season is then calculated using the full MODIS time series. We restricted ourselves to data from the central 50% of the MODIS scan to maximize the spatial resolution of the measurements, providing a final temporal resolution of 3 days. As ETM+ and MODIS are spectrally similar, and to enable a more targeted analysis subset, only index methods that achieved an M-statistic greater than the arbitrary value of 1.5 during the ETM+ analysis (tables 3 and 4) were considered for application to MODIS. Linear spectral unmixing was also applied to the MODIS dataset, where again a series of burned area maps using charcoal thresholds from $>100\%$ to $>45\%$, in increments of 5%, were derived.

5. Results

5.1 *Field and Landsat scales*

Table 2 shows the results of applying the M-statistic to the field spectra convolved to the ETM+ wavelengths. MIRBI performs significantly better than all other methods, with the next best discriminator being the NIR band alone, followed by the Char-Scar index (CSI). The BAI, EVI, GEMI, NDVI, NBR and SAVI indices perform poorly and provide a lower degree of spectral separation than many of the individual ETM+ bands (table 2). Table 3 shows the results of the M-statistic, k statistic and overall accuracy, a, to the ETM+ classifications of Chobe National Park. In terms of spectral separability, the field observations in general showed similar results to ETM+, with the individual ETM+ bands 3 and 4 providing an

Table 2. Separability statistics for simulated and real Landsat ETM+ wavebands.

(*a*) Tests for separability between the field reflectance convolved to the Landsat 7 ETM+ wavebands of burned and unburned surfaces measured within Chobe National Park

Method	*M*-statistic	Method	*M*-statistic
Band 1	0.40	BAI	0.47
Band 2	0.76	CSI	1.64
Band 3	1.09	EVI	0.25
Band 4	1.97	GEMI	0.88
Band 5	1.42	MIRBI	3.78
Band 7	0.67	NBR	1.35
		NDVI	0.01
		SAVI	0.52

(*b*) Changes in mean differences of the burned and unburned surfaces and changes in the standard deviation sums between the simulated and real ETM+ band values

	Mean difference		Standard deviation sum	
	Simulated	Real	Simulated	Real
Band 1	2.99	4.86	7.56	5.69
Band 2	7.14	7.76	9.34	5.84
Band 3	13.78	15.71	12.63	10.61
Band 4	28.87	20.24	14.63	9.55
Band 5	29.90	16.91	21.11	19.66
Band 7	12.14	7.76	18.17	29.66

Table 3. Separability and classification statistics for various burned area mapping methods applied to Landsat 7 ETM+ imagery of Chobe National Park, Botswana.

	Statistics		
Single bands	*M*	*k*	*a*
ETM+ band			
1	0.86	0.23	53.27
2	1.33	0.62	81.21
3	1.48	0.73	87.30
4	2.12	0.95	97.61
5	0.86	0.16	49.42
6	1.61	0.91	95.88
7	0.26	0.05	30.69
Indices			
BAI	1.11	0.92	95.59
CSI	2.18	0.95	97.82
EVI	0.20	0.05	39.27
GEMI	1.40	0.76	89.03
MIRBI	1.76	0.88	94.97
MIRBI (>3.0)	n/a	0.89	95.22
NBR	2.17	0.95	97.75
NDVI	0.24	0.00	20.06
SAVI	0.05	0.01	66.69
VI6T	1.42	0.85	93.56

M denotes the *M*-statistic as defined by Kaufman and Remer (1994) and Pereira (1999).
k denotes the kappa statistic as defined by Foody (2002).
a denotes the overall classification accuracy as defined by Hann *et al.* (2003).
MIRBI was classified by mean ± 2 standard deviations and with a threshold >3.0.

Table 4. Separability and classification statistics for various 3D burned area mapping methods applied to Landsat 7 ETM+ imagery of Chobe National Park, Botswana.

	Statistics			
Index	*M*	*k*	*a*	
CSIT	2.43	0.91	96.22	
NBRT	1.37	0.15	49.35	
NDVIT	0.61	0.00	32.97	
SAVIT	2.06	0.94	97.54	
Methods using >3 bands				
		k	*a*	Reference
Supervised maximum likelihood				
	0.99	99.64	n/a	
ISODATA		0.02	36.77	Ball and Hall (1965)
Charcoal fraction threshold				Settle and Drake (1993)
>100%		0.05	68.46	
>95%		0.28	74.36	
>90%		0.56	83.21	
>85%		0.71	88.42	
>80%		0.79	91.26	
>75%		0.86	94.02	
>70%		0.93	96.81	
>65%		0.96	98.23	
>60%		0.97	98.75	
>55%		0.98	99.11	
>50%		1.00	99.58	
>45%		0.98	99.00	

improved classification over the index methods of BAI, EVI, GEMI, NDVI and SAVI. At the Landsat scale, the highest degree of spectral separability ($M>2$) was attained using CSI, NBR and band 4, respectively. Each of these indices also attained $k=0.95$ and $a=0.97$, although BAI and band 6 also obtained comparable k and a values. The inclusion of the Landsat ETM+ band 6 information within the spectral indices (i.e. VI6T, CSIT, NDVIT and SAVIT) improved the results for all methods, except NBRT (table 4).

These results (tables 2–4) demonstrate that transfer of the analysis from the field to the ETM+ spatial scale resulted, in general, in higher *M*-values. Although bands 5 and 7, MIRBI and SAVI each experienced a decrease in *M* of more than 40%, most indices increased their *M*-statistic. These differences are potentially the result of the increased spatial mixing of individual surface components within the 900 m^2 field of view of the real ETM+ pixels, as opposed to the more limited mixing of different components possible within the small (11 cm^2) ground field of view of the *in situ* spectral measurements. In the latter case, many samples will have contained close to 100% cover of one of the surface components, whereas this is unlikely in the real ETM+ image pixels. This results in the standard deviation, which is included in the denominator of the *M*-statistic (equation (1)), being higher for the simulated ETM+ data than for the real ETM+ data, because in the latter much more spatial averaging of components occurs within each sample. Table 2(*b*) confirms that the sums of the standard deviations for each individual ETM+ band were mainly higher for the simulated data compared to the real data. The only band that exhibited a contrary trend was band 7. Table 2(*b*) further demonstrates that both the green and

red mean differences exhibit no discernable change, while the differences in the means from the simulated to real ETM+ values decrease for bands 4–7. These differences between the VIS and SWIR bands could account for the decrease in spectral separability observed in MIRBI, which could be due to increased variability due to increased contributions of soil and charcoal cover at the scale of the Landsat pixel compared to the relatively pure ground measures.

Of the multispectral classification techniques, the maximum likelihood classification (table 4) achieved a considerably higher accuracy than the index-based methods, and indeed produced the highest classification accuracy of any method. Substantially lower accuracies were obtained using ISODATA (table 4). Linear spectral unmixing using the charcoal fraction threshold produced results strongly dependent on the threshold selected. Thresholds >50% (table 4; figure 2) produced k and a values almost identical to those of maximum likelihood. Comparison of the >50% charcoal fraction map with a false colour composite designed to highlight burnt areas (i.e. RGB: 743) illustrated that, contrary to most other linear spectral unmixing studies (Caetano *et al.* 1996, Vafeidis and Drake 2005), the map appeared to show low errors of commission (figure 2). We compared the >50% charcoal fraction map with this false colour composite solely for a visual assessment of its performance, as the results in tables 2 and 3 already illustrate that this method outperforms comparable approaches such as that produced using a maximum likelihood classifier. Use of this relatively high threshold minimizes errors associated with confusion between charcoal and minor dark soil fractions or shade, provided such contributions occupy less than half a pixel.

Although the mixture modelling using the charcoal fraction map (>50%) showed similar accuracy to the maximum likelihood classifier, the latter approach offers the advantages that the endmembers of charcoal, green vegetation and senesced vegetation are generic to most fire-affected grassland and savannah environments (Elvidge 1990, Smith *et al.* 2005*b*) and that, following endmember selection, no training data are required. As such, the charcoal fraction map method (with the

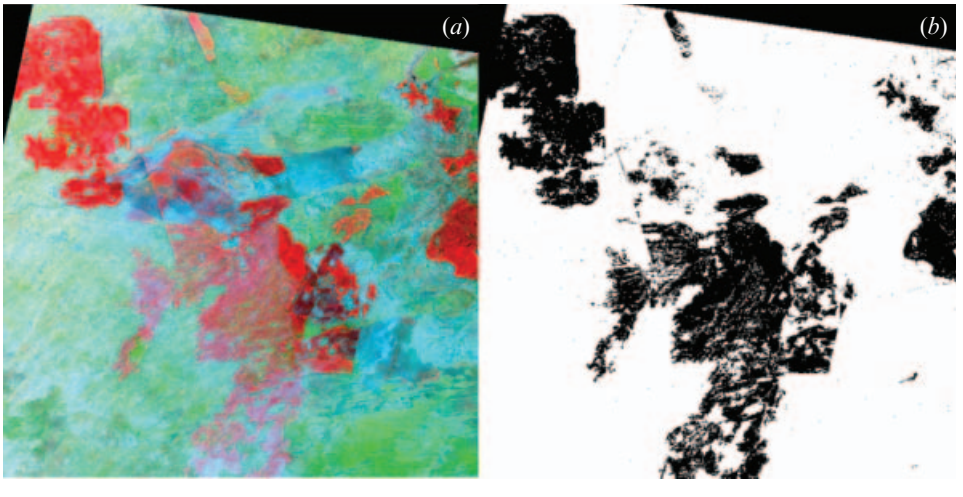

Figure 2. Comparison of (*a*) Landsat ETM+ false colour composite (RGB=7,4,3) highlighting burned areas in Chobe National Park (acquired 8 October 2001), with (*b*) Landsat ETM+ reference image produced using a charcoal mixture map fraction threshold of >50%.

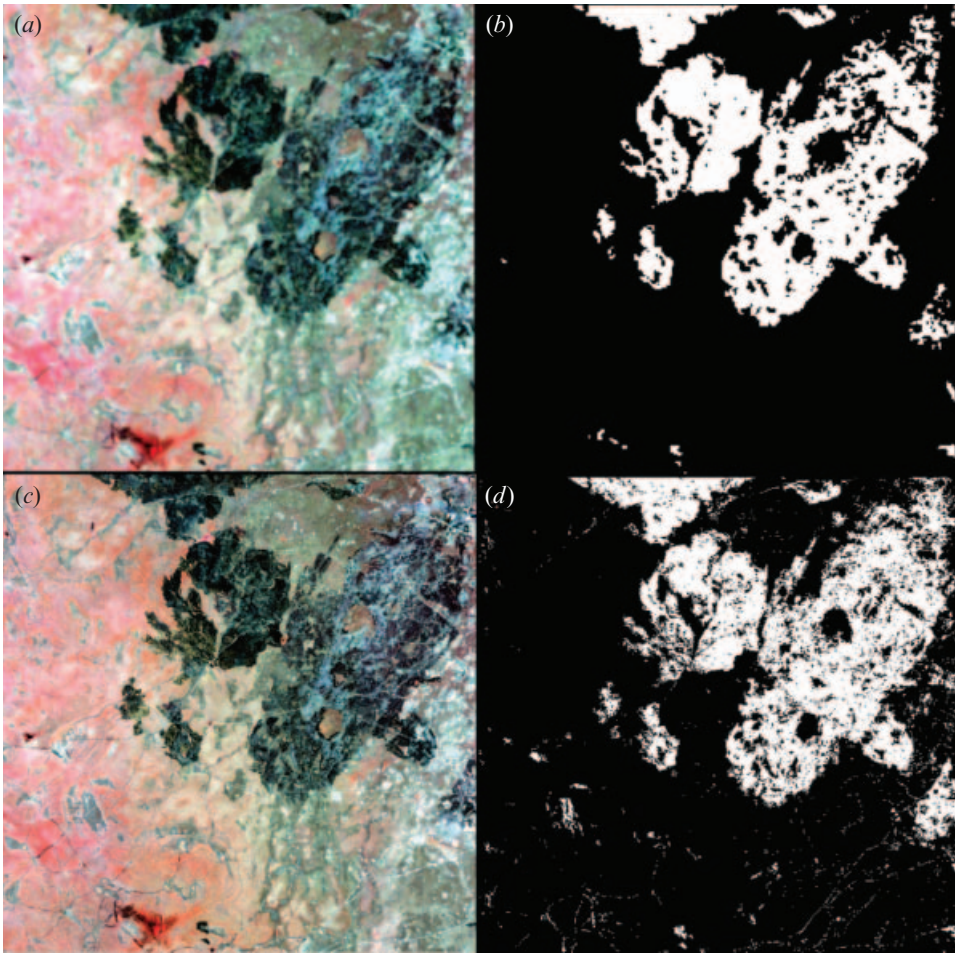

Figure 3. Comparison of burned areas observed surrounding Mongu, Zambia, on 16 August 2000 by Landsat ETM+ (*a*,*b*) and on 17 August 2000 by IKONOS (*c*,*d*). Each of *a* and *c* is an RGB=NIR,R,G false colour composite. (*b*) Landsat ETM+ burned area map produced using a charcoal mixture map threshold of >50%. (*d*) IKONOS burned area reference map produced using a supervised classification with charcoal, senesced vegetation and green vegetation pixels.

>50% charcoal fraction threshold) was identified as the best method to produce the Landsat ETM+ reference image of burned area. This method was therefore further applied to the Landsat image of Mongu and compared to the IKONOS supervised classification of the same area (figure 3). The low commission errors observed with linear spectral unmixing are highlighted in figure 3(*b*), contrasting with the supervised classification of the IKONOS image, which misallocates roads and areas of bare soil as burned (figure 3(*d*)). The ETM+ >50% charcoal map of the Mongu area contains fewer of these misclassifications (figure 3(*b*)) and this is probably the result of the relatively basic spectral coverage provided by the IKONOS imagery (VIS–NIR) compared to that of ETM+, which extends into the SWIR. Even with these uncertainties, for the purpose of this study we considered the higher spatial resolution IKONOS image to represent the truth in the comparison with the Landsat ETM+ classification. This comparison yielded an

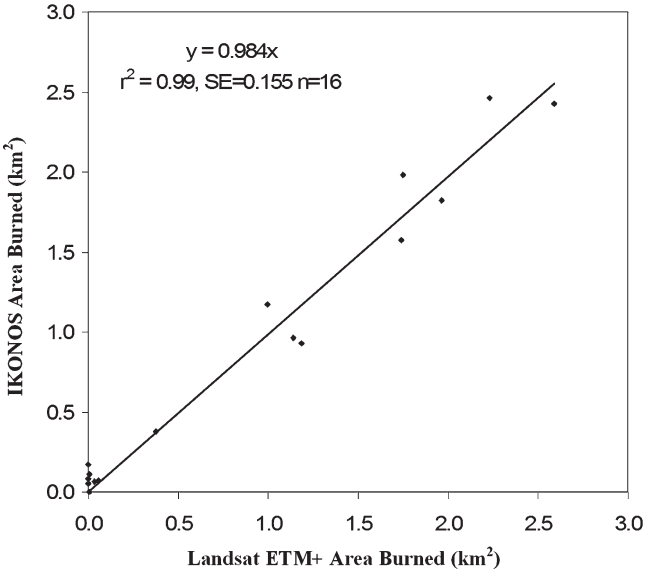

Figure 4. Regression of IKONOS and Landsat area burned for 16 regular grid squares derived from figure 3(*b*) and (*d*). Line of best fit is depicted and regression was significant at the 95% confidence level.

overestimation of burned area by only 1.6%, with a high correspondence and low standard error (figure 4; $r^2=0.99$, SE$=0.155\,km^2$).

5.2 *MODIS scale burnt area estimates*

The result of each of the methods applied to the MODIS imagery are shown in table 5. All performed reasonably well, with *M*-statistics exceeding 1.4 and $r^2>0.69$ and standard error $<131\,km^2$. Table 5 demonstrates that linear spectral unmixing with a fixed threshold charcoal fraction map performed best with a threshold of >65%, but that even at this optimal threshold ($r^2=0.95$, SE$=59.14$) it was less effective than both MIRBI and the maximum likelihood supervised classification.

In the analysis of the index methods, MIRBI attained the highest separability ($M>2.7$). Application of the thermally enhanced spectral indices of CSIT and SAVIT to the MODIS data resulted in a lowering of the *M*-statistic by 0.5 when compared to the Landsat ETM+ analysis. This may be explained by the thermal response of the burned pixels being averaged into too many adjacent non-burned pixels. Comparison of CSI with CSIT at the MODIS scale demonstrates that only a marginal classification improvement is obtained by incorporating this thermal information. At all scales, use of the simple maximum likelihood classifier produces consistently high results, with near perfect accuracy with ETM+, and even with MODIS the approach still provides a highly accurate classification.

To test the appropriateness of the MIRBI threshold of 1.7 recommended by Trigg and Flasse (2001), a range of other thresholds was investigated (table 5). A slightly increased threshold of 1.75 was determined to exhibit the optimal balance of under/overestimation (given by the slope: 0.985), r^2 (0.95) and SE (61.40), indicating that the recommendation of Trigg and Flasse (2001) is very appropriate to our study area (which is within a very similar environment to their Namibian field site). As MIRBI was one of the most accurate methods and does not require either training or field

Table 5. Separability statistics for various burned area mapping methods applied to MODIS imagery of Chobe National Park, Botswana. Comparison of MODIS and Landsat ETM measures of burned area (km^2) performed by a linear regression with no intercept. All relationships are significant at the 95% confidence level.

	Statistics			
Method	*M*	Slope	r^2	SE
Methods using one band				
ρ_{NIR} only	1.61	0.769	0.890	88.59
TIR only	1.66	0.614	0.817	114.55
Methods using two bands				
MIRBI				
No threshold	2.77			
>2.2		1.753	0.669	153.91
>2.1		1.469	0.760	131.20
>2.0		1.252	0.814	115.25
>1.9		1.135	0.875	94.45
>1.8		1.030	0.928	71.67
>1.75		0.985	0.947	61.40
>1.7		0.948	0.960	53.63
>1.6		0.883	0.974	42.79
NBR	2.07	0.744	0.909	80.66
CSI	1.74	0.812	0.914	78.53
Methods using three or more bands				
SAVIT	1.57	0.731	0.888	89.69
CSIT	2.03	0.798	0.929	71.33
Maximum likelihood (all)				
	n/a	0.775	0.960	53.24
Linear spectral unmixing				
Charcoal fraction threshold				
>100%		NS		
>95%		NS		
>90%		NS		
>85%		11.64	0.671	153.52
>80%		3.192	0.657	156.76
>75%		1.526	0.654	157.27
>70%		1.151	0.838	107.47
>65%		0.871	0.951	59.14
>60%		0.630	0.891	88.24
>55%		0.377	0.695	147.83
>50%		0.242	0.563	176.96
>45%		0.208	0.531	183.27

data, it was selected as the method to be applied to the MODIS time series. Using this approach we derived a series of burned area maps to illustrate the progression of fire throughout the 2001 fire season (figures 5(*a*) and 5(*b*)). The total area burned in northern Botswana during this period was 10 267 km^2.

6. Discussion

Our MODIS burnt area estimates appear reasonable given that the Botswana government state that between 8000 and 90 000 km^2 of Botswana burns annually (Flasse *et al.* 2004), and that the GBA2000 burned area map indicates a total burned area of 33 556 km^2 for 2000. Our results show that during the first half of the 2001

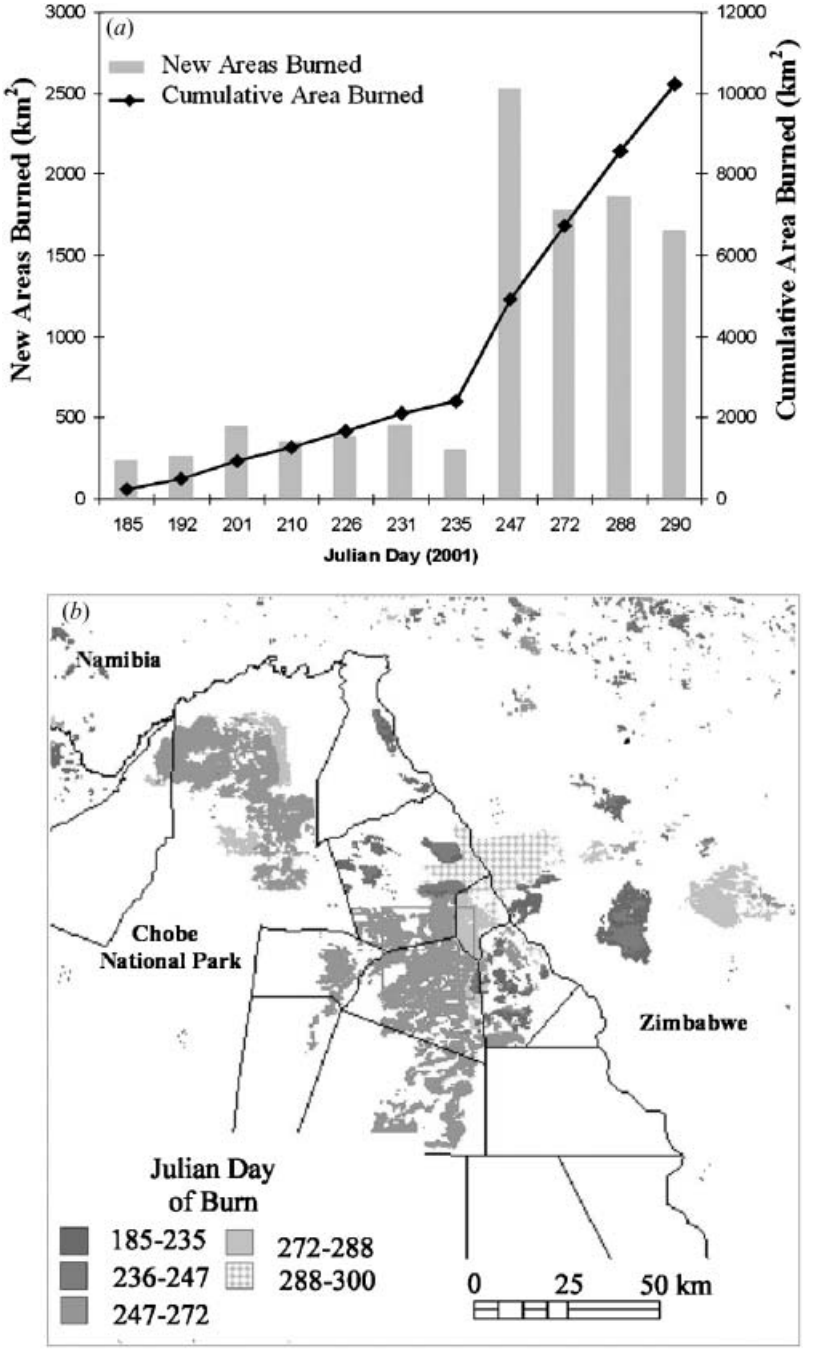

Figure 5. Area burned within the study region (derived from MODIS) during 2001. (*a*) Graph of individual and cumulative burned areas, and (*b*) map of the individual burns and their temporal distribution. Green lines mark the administrative boundaries within Botswana. The total area burned is 10 267 km^2.

dry season (June–August), numerous individual smaller fires each burned significantly less than 1000 km^2 and affected a total area of 2422 km^2. In the second half of the dry season (September–November), there was a significant change in fire behaviour and a series of individual fires each greater than 1000 km^2 in area burned 7845 km^2 total. Therefore, a few large fires are responsible for the majority of the area burned, a phenomenon noted previously in other ecosystems (Kasischke and French 1995, Keeley *et al.* 1999, Stocks *et al.* 2003).

Spectral indices that incorporate the SWIR wavelengths (i.e. CSI, NBR and MIRBI) perform better than indices that only include the NIR and visible bands (i.e. BAI, EVI, GEMI, NDVI and SAVI). However, the spectral separability of these NIR- and visible-based indices were still less than that achieved by the NIR band alone. Thus, for sensors where SWIR reflectance information is not available (e.g. IKONOS), data from the NIR channel alone should be used to map burned area. This is partly in agreement with prior studies in other environments that have highlighted that the NIR band alone generally outperforms spectral indices and other individual bands (Pereira 1999). When using a single band, it is also possible that a threshold-based approach could be enhanced by use of textural information (Smith *et al.* 2002, Hudak and Brockett 2004). Inclusion of the thermal band within the spectral indices produced mixed results. Although $M>2$ for both CSIT and SAVIT, this was confounded by a drastic decline in both k and a. This might have resulted because some validation pixels did not share the emittance properties expected in the burned and unburned surfaces, perhaps due to the inclusion of water holes and large soil patches in the unburned surfaces.

The MIRBI was originally specified by the analysis of field spectra convolved to the ETM+ wavelengths (Trigg and Flasse 2001), an approach replicated in the current study. Trigg and Flasse (2001) showed that the simulated ETM+ band 5 and 7 band reflectance values, when plotted in bispectral feature space, clearly separated burned and unburned surfaces, and this is also the case with the simulated ETM+ data acquired here (figure 6). However, when using the real ETM+ data, some feature space overlap between burned and unburned pixels occurs (figure 6), and this effect, along with the related lowering of the M-statistic (tables 1 and 2), is due to the presence of increased numbers of mixed pixels within the real ETM+ imagery (i.e. those containing a mixture of burned and unburned surfaces, for example those at the edge of the fire-affected area) when compared to the simulated ETM+ data. These bispectral plots also highlight the apparent improvement in the spectral separability at both field and satellite scales observed using ETM+ bands 5 and 7 (MIRBI), compared to ETM+ bands 4 and 7 (CSI and NBR).

In general, at both the field and satellite scales, inclusion within the spectral indices of either the SWIR or TIR information alongside the NIR (i.e. MIRBI, VI6T, CSI, CSIT, NBR, NBRT and SAVIT) provide the greatest class separability. This concurs with previous studies indicating that techniques using a combination of NIR with SWIR and/or thermal bands are well suited to discriminating burned and unburned savannah areas (Eva and Lambin 1998, Trigg and Flasse 2001, Holden *et al.* 2005).

Overall, the usage of linear spectral unmixing to map burned areas within such environments shows promise. However, these results demonstrated that using a charcoal fraction map with a fixed threshold (>50% in this case) was unstable with respect to a change of scale from ETM+ to MODIS. However, application of >65% threshold at both the TM and MODIS scales would produce consistently high accuracy burned area maps (tables 4 and 5). The loss of performance between use of

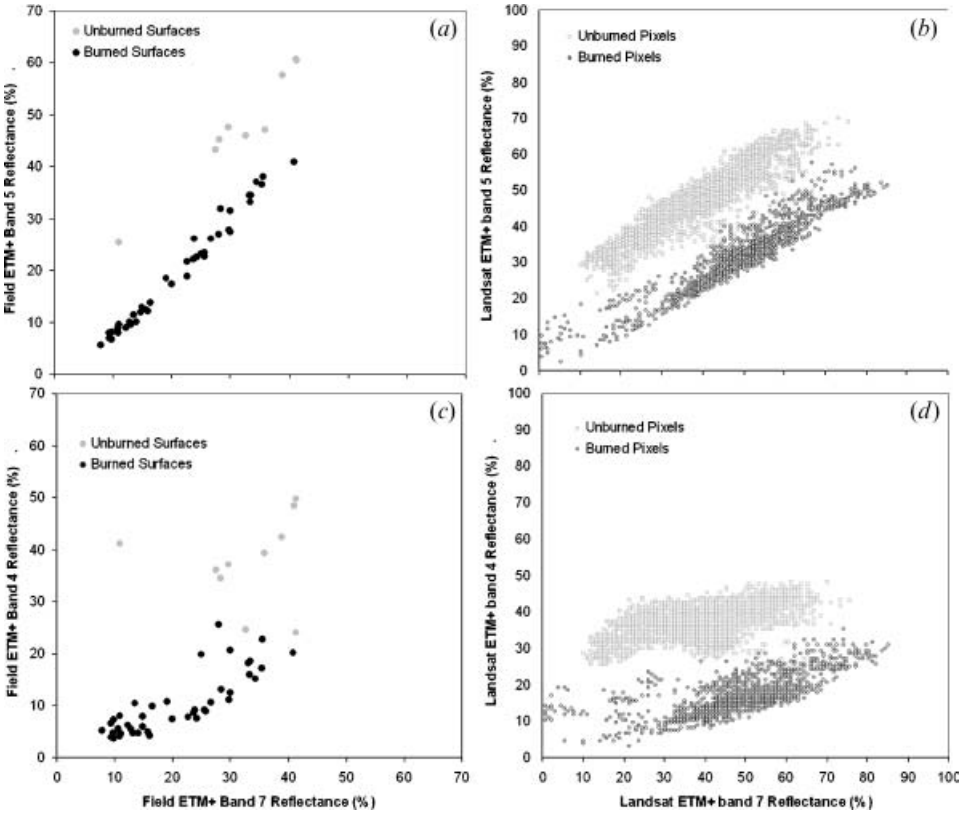

Figure 6. Landsat 7 ETM+ bispectral reflectance plots of burned and unburned surfaces. (*a*) Simulated ETM+ band 5 and 7 reflectance values derived from *in situ* surface spectral measurements made in the field. (*b*) Real ETM+ band 5 and 7 reflectance values derived from ETM+ imagery. (*c*) Simulated ETM+ band 4 and 7 reflectance values derived from surface spectral measurements. (*d*) Real ETM+ band 4 and 7 reflectance values derived from Landsat ETM+ imagery. Note that in (*a*) and (*c*) a clear boundary exists between the surfaces and the ground reflectances but at the satellite level this boundary is less distinct.

the ETM+- and MODIS-derived charcoal fraction maps is most probably due to the decrease in signal to noise, to which linear spectral unmixing is sensitive (Drake *et al.* 1999). As linear spectral unmixing requires a lower degree of *a priori* information than does the supervised maximum likelihood approach, the former method is more suitable for multiscale assessment of area burned. Furthermore, application of the charcoal fraction information could provide additional information relating to the immediate post-fire effects, such as vegetation mortality and potential recovery, which are important variables for monitoring long-term carbon accumulation (Lentile *et al.* 2006).

7. Conclusion

This study has evaluated, for southern African savannah environments, the most suitable method to produce a burned area reference map from Landsat ETM+ imagery for use as a surrogate to ground truth data when validating lower spatial resolution burned area estimates derived from sensors such as MODIS. At the ETM+ scale, the application of multiband supervised classification that relies on

training data, although an improvement over single band or index-based measures, was less effective than maps produced by a fixed threshold based on the charcoal fraction map derived from mixture modelling. The charcoal fraction map method developed here uses only the generic savannah endmembers of charcoal, senesced vegetation and green vegetation and therefore could be applied directly to imagery of similar spatial resolution to ETM+. However, the more widespread utility of the method at other spatial scales appears questionable, given its poor performance when used with MODIS. The most effective method for use with MODIS was found to be the MIRBI, segmented with a fixed threshold of 1.75. This confirms the basic utility of the MIRBI approach for savannah burned area mapping, as presented by Trigg and Flasse (2001).

Although these results are likely to be valid in other savannah or potentially in similar semi-arid environments, further research is required in other fire-prone environments, such as boreal and temperate forests. Following recent conclusions by Lentile *et al.* (2006) and the results of the current study, we reiterate the need for studies to comprehensively evaluate the efficacy of burned area mapping methods in more than one study region or ecosystem type. By contrast, future studies should seek to evaluate methods that are relevant to fires occurring globally. In this vein, new approaches to burned area mapping are becoming available, including those that use large time-series to detect the step-changes in reflectance that are expected on burning (Roy *et al.* 2006). This research into optimal methods and their relative accuracy should therefore be revisited when the development of these new approaches reaches stability, as they offer the prospect of automated burned area mapping across the African continent with little operator involvement.

Acknowledgements

Alistair Smith was supported by the NERC/GANE Thematic Program studentship (NER/S/R/2000/04057). Special thanks to Karen Anderson and the staff of the NERC/EPFS equipment pool for field spectrometry for use of the GER-3700 spectrometer. Alistair Smith is currently part of the Forest Public Access Resource Center (ForestPARC) and is supported with funding from the Upper Midwest Aerospace Consortium (UMAC), which is in turn supported with funds from NASA. MODIS data were acquired as part of NASA's Earth Science Enterprise with algorithms developed by the MODIS Science Teams. Partial funding for this research was provided by the USDA/USDI Joint Fire Sciences Program (Projects 05-4-1-07 and 05-2-1-101). The MODIS data were archived and distributed by the Goddard DAAC. We thank the editor and the anonymous reviewers for their advice and suggestions in improving this paper.

References

Andreae, M.O. and Merlet, P., 2001, Emission of trace gases and aerosols from biomass burning. *Global Biochemical Cycles*, **15**, pp. 955–966.

Ball, G.H. and Hall, D.J., 1965, ISODATA, a novel method of data analysis and pattern classification. Technical Report, Stanford Research Institute, Melo Park, CA, USA.

Barbosa, P.M., Pereira, J.M.C. and Grégoire, J.-M., 1998, Composting criteria for burned area assessment using multitemporal low resolution satellite data. *Remote Sensing of Environment*, **65**, pp. 38–49.

Barbosa, P.M., Grégoire, J.-M. and Pereira, J.M.C., 1999, An algorithm for extracting burned areas from time series of AVHRR GAC data applied at a continental scale. *Remote Sensing of Environment*, **69**, pp. 253–263.

Brivio, P.A., Maggi, M., Binaghi, E. and Gallo, I., 2003, Mapping burned surfaces in Sub-Saharan Africa based on multi-temporal neural classification. *International Journal of Remote Sensing*, **24**, pp. 4003–4018.

Caetano, M., Mertes, L., Cadete, L. and Pereira, J., 1996, Assessment of AVHRR data for characterizing burned areas and post-fire vegetation recovery. *EARSeL Advances in Remote Sensing*, **4**, pp. 124–134.

Chander, G. and Markham, B., 2003, Revised Landsat-5 TM radiometric calibration procedures and postcalibration dynamic ranges. *IEEE Transactions on Geoscience and Remote Sensing*, **41**, pp. 2674–2677.

Chen, X., Vierling, L., Rowell, E. and Defelice, T., 2004, Using lidar and effective LAI to evaluate IKONOS and Landsat 7 ETM+ vegetation estimates in a ponderosa pine forest. *Remote Sensing of Environment*, **91**, pp. 14–26.

Chuvieco, E., Martín, M.P. and Palacios, A., 2002, Assessment of different spectral indices in the red–near-infrared spectral domain for burned land discrimination. *International Journal of Remote Sensing*, **23**, pp. 5103–5110.

Cochrane, M.A. and Souza, C.M., 1998, Linear mixture model classification of burned forests in the Eastern Amazon. *International Journal of Remote Sensing*, **19**, pp. 3433–3440.

Cofer, W.R., III., Levine, J.S., Winstead, E.L., Cahoon, D.R., Sebacher, D.I., Pinto, J.P. and Stocks, B.J., 1996, Source compositions of trace gases released during African savanna fires. *Journal of Geophysical Research*, **101**, pp. 23597–23602.

Crutzen, P.J. and Andreae, M.O., 1990, Biomass burning in the tropics: impact on atmospheric chemistry and biogeochemical cycles. *Science*, **250**, pp. 1669–1678.

Drake, N.A. and White, K., 1991, Linear mixture modelling of Landsat Thematic Mapper data for mapping the distribution and abundance of gypsum in the Tunisian Southern Atlas. In *Spatial Data 2000: Proceedings of a Joint Conference of the Photogrammetric Society, the Remote Sensing Society, the American Society for Photogrammetry and Remote Sensing, Christ Church, Oxford*, I. Dowman (Ed.), pp. 168–177 (London: Department of Photogrammetry and Surveying, University College London).

Drake, N.A., Mackin, S. and Settle, J.J., 1999, Mapping vegetation, soils, and geology in semiarid shrublands using spectral matching and mixture modelling of SWIR AVIRIS imagery. *Remote Sensing of Environment*, **67**, pp. 12–25.

Elvidge, C.D., 1990, Visible and near infrared reflectance characteristics of dry plant materials. *International Journal of Remote Sensing*, **11**, pp. 1775–1795.

Eva, H. and Lambin, E.F., 1998, Burnt area mapping in Central Africa using ATSR data. *International Journal of Remote Sensing*, **19**, pp. 3473–3497.

Fernandez, A., Illera, P. and Casanova, J.L., 1997, Automatic mapping of surfaces affected by forest fires in Spain using AVHRR NDVI composite image data. *Remote Sensing of Environment*, **60**, pp. 153–162.

Flasse, S.P., Trigg, S.N., Ceccato, P.N., Perryman, A.H., Hudak, A.T., Thompson, M.W., Brockett, B.H., Drame, M., Ntabeni, T., Frost, P.E., Landmann, T. and Le Roux, J.L., 2004, Remote sensing of vegetation fires and its contribution to a fire management information system. In *Wildland Fire Management Handbook for Sub-Sahara Africa*, J.G. Goldammer and N. de Ronde (Eds), pp. 158–211 (The Hague: BBP Academic Publishers, 2004).

Flemming, D., 2003, Ikonos DN value conversion to planetary reflectance, Version 2.1, Commercial Remote Sensing for Earth Systems Science (CRESS), University of Maryland. Available online at: www.geog.umd.edu/cress/papers/guide_dn2pr.pdf (accessed 3 November 2004).

Foody, G.M., 2002, Status of land cover classification accuracy assessment. *Remote Sensing of Environment*, **80**, pp. 185–201.

Frederiksen, P., Langass, S. and Mbaye, M., 1990, NOAA AVHRR and GIS-based monitoring of fire activity in Senegal – a provisional methodology and potential

applications. In *Fires in the Tropical Biota, Ecological Studies 82*, J.G. Goldammer (Ed.), pp. 400–417 (Berlin: Springer).

FRENCH, N.H.F., GOOVAERTS, P. and KASISCHKE, E.S., 2004, Uncertainty in estimating carbon emissions from boreal forest fires. *Journal of Geophysical Research*, **109**, D14208, doi:10.1029/2003JD003635.

FULLER, D.O. and FALK, M., 2001, Burned area in Kalimantan, Indonesia mapped with NOAA-AVHRR and Landsat TM imagery. *International Journal of Remote Sensing*, **22**, pp. 691–697.

GOLDAMMER, J.G., 1999, Forests on fire. *Science*, **284**, pp. 1782–1783.

GRÉGOIRE, J.-M., TANSEY, K. and SILVA, J.M.N., 2003, The GBA2000 initiative: developing a global burned area database from SPOT-VEGETATION imagery. *International Journal of Remote Sensing*, **24**, pp. 1369–1376.

HANN, D.B., SMITH, A.M.S. and POWELL, A.K., 2003, Technical Note: Classification of off-diagonal points in a co-occurrence matrix. *International Journal of Remote Sensing*, **24**, pp. 1949–1956.

HAO, W.M., LUI, M.-H. and CRUTZEN, P.J., 1990, Estimates of annual and regional releases of CO2 and other trace gases to the atmosphere from fires in the tropics, based on the FAO statistics for the period 1975–1980. In *Fire in the Tropical Biota: Ecosystem Processes and Global Challenges, Ecological Studies 84*, J.G. Goldammer (Ed.), pp. 440–462 (New York: Springer-Verlag, 1990).

HAO, W.M. and LUI, M.-H., 1994, Spatial and temporal distribution of tropical biomass burning in 1980 with $5^\circ \times 5^\circ$ resolution. *Global Biochemical Cycles*, **8**, pp. 495–503.

HELY, C., ALLUEATME, S., SWAP, R.J., SHUGART, H.H. and JUSTICE, C.O., 2003a, SAFAI-2000 characterization of fuels, fire behavior, combustion completeness, and emissions from experimental burns in infertile grass savannas in western Zambia. *Journal of Arid Environments*, **54**, pp. 381–394.

HELY, C., DOWTY, P.R., ALLEAUME, S., CAYLOR, K.K., KORONTZI, S., SWAP, R.J., SHUGART, H.H. and JUSTICE, C.O., 2003b, Regional fuel load for two climatically contrasting years in southern Africa. *Journal of Geophysical Research*, **108**, 8475, doi:10.1029/2002JD002341.

HUETE, A.R., LIU, H.Q., BATCHILY, K. and VAN LEEUWEN, W., 1997, A comparison of vegetation indices over a global set of TM images for EOS-MODIS. *Remote Sensing of Environment*, **59**, pp. 440–451.

HOLDEN, Z., SMITH, A.M.S., MORGAN, P., ROLLINS, M.G. and GESSLER, P.E., 2005, Comparison of Landsat-derived fire perimeters with fire atlas data: evaluation of existing and thermally enhanced spectral indices. *International Journal of Remote Sensing*, **26**, pp. 4801–4808.

HUDAK, A.T. and BROCKETT, B.H., 2004, Mapping fire scars in a southern African savannah using Landsat imagery. *International Journal of Remote Sensing*, **25**, pp. 3231–3243.

KASISCHKE, E.S. and BRUHWILER, L.P., 2003, Emissions of carbon dioxide, carbon monoxide, and methane from boreal forest fires in 1998. *Journal of Geophysical Research*, **108**, D13, 8146, doi:10.1029/2001JD000461.

KASISCHKE, K.S. and FRENCH, N.H.F., 1995, Locating and estimating the aerial extent of wildfires in Alaskan boreal forests using multiple-season AVHRR NDVI composite data. *Remote Sensing of Environment*, **51**, pp. 263–275.

KAUFMAN, Y.J. and REMER, L.A., 1994, Detection of forests using mid-IR reflectance: an application for aerosol studies. *IEEE Transactions on Geoscience and Remote Sensing*, **32**, pp. 672–683.

KEELEY, J.K., FOTHERINGHAM, C.J. and MORAIS, M., 1999, Re-examining fire suppression impacts on brushland fire regimes. *Science*, **284**, pp. 1829–1832.

KEY, C.H. and BENSON, N.C., 2002, Measuring and remote sensing of burn severity. In *U.S. Geological Survey Wildland Fire Workshop*, 31 October–3 November 2000, Los Alamos, NM (USGS Open-File Report 02-11), p. 55.

KRUSE, F.A., KIEREIN-YOUNG, K.S. and BOARDMAN, J.E., 1990, Mineral mapping at Cuprite, Nevada with a 63-channel imaging spectrometer. *Photogrammetric Engineering and Remote Sensing*, **56**, pp. 83–92.

LANDMANN, T., 2003, Characterizing sub-pixel Landsat ETM+ fire severity on experimental fires in the Kruger National Park, South Africa. *South African Journal of Science*, **99**, pp. 357–360.

LENTILE, L.B., HOLDEN, Z.A., SMITH, A.M.S., FALKOWSKI, M.J., HUDAK, A.T., MORGAN, P., GESSLER, P.E. and BENSON, N.C., 2006, Remote sensing techniques to assess active fire and post-fire effects. *International Journal of Wildland Fire*, **15**, pp. 319–345.

LEVINE, J.S., 1990, Burning trees and bridges. *Nature*, **346**, pp. 511–512.

LEWIS, S.A., WU, J.Q. and ROBICHAUD, P.R., 2006, Assessing burn severity and comparing soil water repellency, Hayman Fire, Colorado. *Hydrological Processes*, **20**, pp. 1–16.

LOPEZ-GARCIA, M.J. and CASELLES, V., 1991, Mapping burns and natural reforestation using Thematic Mapper data. *Geocarto International*, **1**, pp. 31–37.

NIELSEN, T.T., MBOW, C. and KANE, R., 2002, A statistical methodology for burned area estimation using multitemporal AVHRR data. *International Journal of Remote Sensing*, **23**, pp. 1181–1196.

PEREIRA, J.M.C., 1999, A comparative evaluation of NOAA/AVHRR vegetation indexes for burned surface detection and mapping. *IEEE Transactions on Geoscience and Remote Sensing*, **37**, pp. 217–226.

PEREIRA, J.M.C., PEREIRA, B.S., BARBOSA, P., STROPPIANA, D., VASCONELOS, M.J.P. and GREGIRE, J.-P., 1999, Satellite monitoring of fire in the EXPRESSO study area during the 1996 dry season experiment: active fires burnt area, and atmospheric emissions. *Journal of Geophysical Research*, **104**, pp. 30701–30712.

PINTY, B. and VERSTRAETE, M., 1992, GEMI: a non-linear index to monitor global vegetation from satellites. *Vegatatio*, **101**, pp. 15–20.

QIN, W. and GERSTL, S.A.W., 2000, 3-D scene modelling of semi-arid vegetation cover and its radiation regime. *Remote Sensing of Environment*, **74**, pp. 145–162.

RAZAFIMPANILO, H., FROUIN, R., IACOBILLIS, S.F. and SOMERVILLE, R.C.J., 1995, Methodology for estimating burned area from AVHRR reflectance data. *Remote Sensing of Environment*, **54**, pp. 273–289.

RICHARDS, J.A. and JIA, X., 1999, *Remote Sensing Digital Image Analysis: An Introduction*, 3rd edn (Berlin: Springer), pp. 278–283.

ROUSE, J.W., JR., HAAS, R.H., DEERING, D.W., SCHELL, J.A. and HARLAN, J.C., 1974, Monitoring the vernal advancement and retrogradation (green wave effect) of natural vegetation. NASA/GSFC Type III Final Report (Greenbelt, MD: NASA).

ROY, D.P. and LANDMANN, T., 2005, Characterizing the surface heterogeneity of fire effects using multi-temporal reflective wavelength data. *International Journal of Remote Sensing*, **26**, pp. 4197–4218.

ROY, D.P., GIGLIO, L., KENDALL, J.D. and JUSTICE, C.O., 1999, Multi-temporal active-fire based burn scar detection algorithm. *International Journal of Remote Sensing*, **20**, pp. 1031–1038.

ROY, D.P., BOSCHETTI, L. and TRIGG, S.N., 2006, Remote sensing of fire severity: assessing the performance of the normalized burn ratio. *IEEE Geoscience and Remote Sensing Letters*, **3**, pp. 112–116.

SA, A.C.L., PEREIRA, J.M.C., VASCONCELOS, M.J.P., SILVA, J.M.N., RIBEIRO, N. and AWASSE, A., 2003, Assessing the feasibility of sub-pixel burned area mapping in miombo woodlands of northern Mozambique using MODIS imagery. *International Journal of Remote Sensing*, **24**, pp. 1783–1796.

SCHOLES, R.J., KENDALL, J. and JUSTICE, C.O., 1996, The quantity of biomass burned in southern Africa. *Journal of Geophysical Research*, **101**, pp. 23667–23676.

SEILER, W. and CRUTZEN, P.J., 1980, Estimates of grass and net fluxes of carbon between the biosphere and the atmosphere from biomass burning. *Climatic Change*, **2**, pp. 207–247.

SETTLE, J.J. and DRAKE, N.A., 1993, Linear mixing and the estimation of ground cover proportions. *International Journal of Remote Sensing*, **14**, pp. 1159–1177.

SHABANOV, N.V., LO, K., GOPAL, S. and MYNENI, R.B., 2005, Subpixel burn detection in Moderate Imaging Spectroradiometer 500-m data with ARTMAP neural networks. *Journal of Geophysical Research*, **110**, D03111, doi:10.1029/2004JD005257.

SILVA, J.M.N., PEREIRA, J.M.C., CABRAL, A.I., SA, A.C.L., VASCONCELOS, M.J.P., MOTA, B. and GREGOIRE, J.-P., 2003, An estimate of the area burned in southern Africa during the 2000 dry season using SPOT-VEGETATION satellite data. *Journal of Geophysical Research*, **108**, 8498, doi:10.1029/2002JD002320.

SLEGERT, F., RUECKER, G., HINRICHS, A. and HOFFMANN, A.A., 2001, Increased damage from fires in logged forests during droughts caused by El Nino. *Nature*, **414**, pp. 437–440.

SMITH, A.M.S., 2004, Determining nitrogen volatilised within African savanna fires via ground-based remote sensing. PhD thesis, University of London.

SMITH, A.M.S. and HUDAK, A.T., 2005, Estimating combustion of large downed woody debris from residual white ash. *International Journal of Wildland Fire*, **14**, pp. 245–248.

SMITH, G.M. and MILTON, E.J., 1999, The use of the empirical line method to calibrate remotely sensed data to reflectance. *International Journal of Remote Sensing*, **20**, pp. 2653–2662.

SMITH, A.M.S., WOOSTER, M.J., POWELL, A.K. and USHER, D., 2002, Texture based feature extraction: application to burn scar detection in Earth observation satellite imagery. *International Journal of Remote Sensing*, **23**, pp. 1733–1739.

SMITH, A.M.S., WOOSTER, M.J., DRAKE, N.A., PERRY, G.L.W. and DIPOTSO, F.M., 2005a, Fire in African savannah: testing the impact of incomplete combustion on pyrogenic emissions estimates. *Ecological Applications*, **15**, pp. 1074–1082.

SMITH, A.M.S., WOOSTER, M.J., DRAKE, N.A., DIPOTSO, F.M., FALKOWSKI, M.J. and HUDAK, A.T., 2005b, Testing the potential of multi-spectral remote sensing for retrospectively estimating fire severity in African savanna environments. *Remote Sensing of Environment*, **97**, pp. 92–115.

STOCKS, B.J., MASON, J.A., TODD, J.B., BOSCH, E.M., WOTTON, B.M., AMIRO, B.D., FALNNIGAN, M.D., HIRSCH, K.G., LOGAN, K.A., MARTELL, D.L. and SKINNER, W.R., 2003, Large forest fires in Canada, 1989–1997. *Journal of Geophysical Research*, **107**, 8149, doi:10.1029/2001JD000484.

STROPPIANA, D., PINNOCK, S., PEREIRA, J.M.C. and GREGOIRE, J.-M., 2002, Radiometric analysis of SPOT-VEGETATION images for burnt area detection in Northern Australia. *Remote Sensing of Environment*, **82**, pp. 21–37.

TRIGG, S. and FLASSE, S., 2000, Characterising the spectral–temporal response of burned savannah using in situ spectroradiometry and infrared thermometry. *International Journal of Remote Sensing*, **21**, pp. 3161–3168.

TRIGG, S. and FLASSE, S., 2001, An evaluation of different bi-spectral spaces for discriminating burned shrub-savanna. *International Journal of Remote Sensing*, **22**, pp. 2641–2647.

VAN WAGTENDONK, J.W., ROOT, R.R. and KEY, C.H., 2004, Comparison of AVIRIS and Landsat ETM+ detection capabilities for burn severity. *Remote Sensing of Environment*, **92**, pp. 397–408.

VAFEIDIS, A.T. and DRAKE, N.A., 2005, A two-step method for estimating the extent of burnt areas with the use of coarse-resolution data. *International Journal of Remote Sensing*, **26**, pp. 2441–2459.

WESSMAN, C.A., BATESON, C.A. and BENNING, T.L., 1997, Detecting fire and grazing patterns in tallgrass prairie using spectral mixture analysis. *Ecological Applications*, **7**, pp. 493–511.